Free Energy Generalization of the Peierls Potential in Iron

M. R. Gilbert,[1] P. Schuck,[2] B. Sadigh,[3] and J. Marian[3,*]

[1]*EURATOM/CCFE Fusion Association, Culham Science Centre, Abingdon, Oxfordshire OX14 3DB, United Kingdom*
[2]*Oak Ridge National Laboratory, Oak Ridge, Tennessee 37831, USA*
[3]*Lawrence Livermore National Laboratory, Livermore, California 94551, USA*

In body-centered-cubic (bcc) crystals, $1/2\langle 111\rangle$ screw dislocations exhibit high intrinsic lattice friction as a consequence of their nonplanar core structure, which results in a periodic energy landscape known as the Peierls potential U_P. The main features determining plastic flow, including its stress and temperature dependences, can be derived directly from this potential, hence its importance. In this Letter, we use thermodynamic integration to provide a full thermodynamic extension of U_P for bcc Fe. We compute the Peierls free energy path as a function of stress and temperature and show that the critical stress vanishes at 700 K, supplying the qualitative elements that explain plastic behavior in the athermal limit.

Dislocations are ubiquitous line defects that mediate plastic deformation in crystalline materials. In body-centered-cubic (bcc) metals, plasticity is governed by the motion of $1/2\langle 111\rangle$ screw dislocations on close-packed planes. Generally, this motion is understood to occur over a periodic energy landscape known as the Peierls potential U_P. Theoretical descriptions of this potential show that it is very stiff in bcc Fe, leading in some cases to critical stresses (those at which the lattice resistance is suppressed) in excess of 1 GPa. However, experimentally, it is found that the flow stress—the macroscopic equivalent of the critical stress—is roughly one-third lower than calculated values. The most convincing explanation for this discrepancy that we possess currently is the contribution of zero-point motion to the Peierls potential at temperatures where quantum effects cannot be neglected [1].

At low stresses, one can safely assume that the Peierls potential remains unchanged and that slip proceeds via the thermally activated nucleation of steps on the dislocation line, known as kink pairs, and their subsequent sideward relaxation. However, at stresses approaching the critical stress, referred to as Peierls stress σ_P at 0 K, it is insufficient to consider only the zero stress internal energy to represent the Peierls trajectory. This trajectory is defined as the rectilinear path, denoted by the reaction coordinate x, between two equivalent equilibrium states (known as "easy core") on the Peierls potential, which has periodicity $h = a_0\sqrt{6}/3$, where a_0 is the lattice constant. Rodney and Proville [2] showed that at moderate to high stresses, the core undergoes internal transformations that modify the Peierls energy landscape. This $U_P(\sigma)$, where σ is the shear stress resolved on a $\{110\}$ plane—applied using the Parrinello-Rahman method [3]—is provided in Fig. 1 using the nudged-elastic-band (NEB) method [4] and a standard semiempirical interatomic force field developed by Mendelev *et al.* [5]. Although this force field yields the nondegenerate screw dislocation core structure, in accordance with density functional theory

(DFT) calculations, it also predicts a metastable split core configuration known now to be an artifact [6]. The Peierls potential is then defined by the system enthalpy $H_P(\sigma) = U_P(\sigma) - W_p$, where W_p is equal to the plastic work associated with the shear strain in the simulation box. For an accurate calculation of W_p, the reaction coordinate must be expressed in terms of the dislocation core position, which is calculated here by matching the atomic displacement field to the Volterra solution for a screw dislocation (see the Supplemental Material [7]). For the model used in Fig. 1, σ_P is approximately 1250 MPa as first computed by Chaussidon *et al.* [8] (DFT calculations: ≈ 1100 to 1400 MPa [9,10]). The inset to Fig. 1 shows the two-dimensional representation of the NEB trajectory at several stresses on the (111) plane using a differential displacement map. The figure shows that as the shear stress increases, the path approaches one of the $\langle 111\rangle$ atomic rows associated
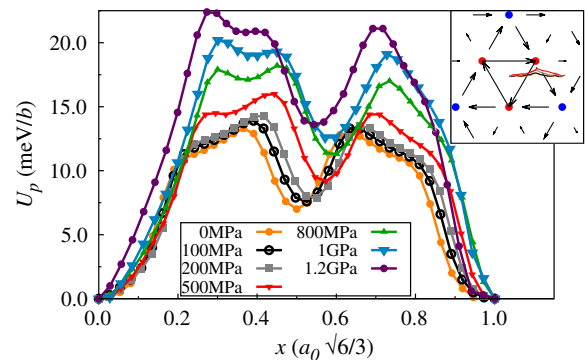

FIG. 1 (color online). Peierls potential U_P as a function of stress for the Mendelev interatomic potential for Fe [5]. x represents the (nondimensional) dislocation core position. Note that DFT calculations predict a sinusoidal profile with an amplitude of $\Delta U_P = 30 \sim 40$ meV/b [10]. The inset to the figure shows the transition path on the (111) plane taken by the dislocation at several values of σ shown in the main figure.

with split core configuration. At zero stress, the transition path is practically rectilinear—consistent with recent DFT calculations [9,10]—which is a manifestation of the structure of the dislocation core energy landscape [11].

Tensile tests place the athermal limit of bcc Fe, i.e., the point at which flow occurs without mechanical aid, at various temperatures between 300 and 400 K [12–17]. This limit is thought to establish the extent of the validity of the classical kink-pair mechanism. Kink-pair energies have been calculated as a function of stress utilizing atomistic and line tension models, all of which make use of a substrate Peierls potential [9,18]. However, despite its importance, the effect of temperature on the Peierls potential has not yet been addressed. In this Letter, we generalize the Peierls enthalpy to finite-temperature conditions by calculating the Gibbs free energy of atomistic Fe systems using a combination of periodic (dipole) and cylindrical configurations containing in excess of $N = 12\,000$ atoms, as described in Refs. [19,20]. Dislocation segments $5b$ in length were considered, where $b = a_0\sqrt{3}/2$ is the Burgers vector's modulus and $a_0 \approx 0.27$ nm. The reference configurations used here are those calculated at constant stress using the NEB method.

Adding T to the natural variables σ and N results in the isothermal-isobaric ensemble, whose characteristic state function is the Gibbs free energy

$$G = H - TS,$$

where S is the entropy, defined in our pure and periodic systems solely by vibrational contributions. Our objective is to establish the importance of incorporating temperature effects into models based on the standard picture of the Peierls potential and to compute explicitly the athermal limit from atomistic calculations. To obtain the Peierls free energy G_P, we equate the Peierls transition path to an activated process described by a general configurational nonlinear many-body reaction coordinate [21]. As a first approximation, we first calculate the harmonic free energy of each configuration along the NEB trajectory as

$$G_i^h(T) = kT \sum_k 2 \sinh\left(\frac{\hbar\omega_i(\mathbf{k})}{2kT}\right), \qquad (1)$$

where $\omega(\mathbf{k})$ are the eigenfrequencies corresponding to eigenvectors $\mathbf{k}$ pertaining to each NEB replica i. However, as Fig. 2 demonstrates, relatively large mean square displacements can be measured already at 100 K along the reaction coordinate, particularly within the initial 15% of the Peierls trajectory. Such anharmonic behavior is a manifestation of a pathology of the Mendelev force field, which results in a transition path at 0 K that may not reflect the true finite-temperature dynamics of the system. G^h has been calculated for comparison (see the Supplemental Material [7]), nonetheless, and following Proville *et al.* [1], to account for zero-point motion at low temperatures. We shall discuss this correction in later paragraphs.
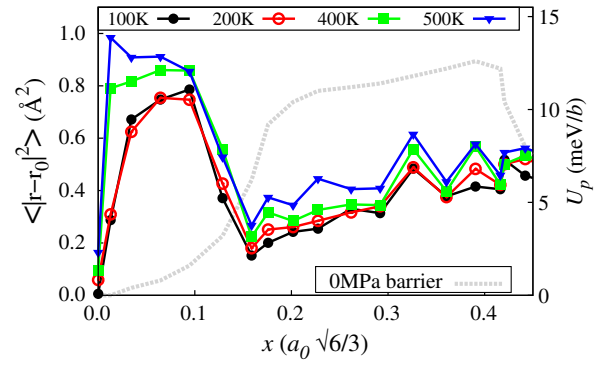

FIG. 2 (color online). Time-averaged atomic mean square displacement along the Peierls trajectory (up to 45% of the reaction coordinate) at zero stress. Areas with large $\langle r^2 \rangle$ indicate anharmonic behavior. The unstressed U_P is shown as a dashed gray line for reference.

Our method to compute full, anharmonic free energies is based on Kirkwood's approximation to obtain the potential of mean force [22]. Assuming a Hamiltonian of the type $\mathcal{H} = \mathbf{p}^2/2m + U(\mathbf{q})$, where $\mathbf{p}$ and $\mathbf{q}$ are the generalized momenta and coordinates, respectively, one can write the Gibbs free energy as

$$G = -\frac{\log \mathcal{Z}}{\beta} = -\frac{1}{\beta}\log\int d\mathbf{q}d\mathbf{p}\,\exp\{-\beta\mathcal{H}(\mathbf{q}, \mathbf{p})\}$$
$$= -\frac{\mathcal{C}}{\beta}\log\int d\mathbf{q}\,\exp\{-\beta U(\mathbf{q})\}, \qquad (2)$$

where $\mathcal{Z}$ is the canonical partition function, $\beta = 1/kT$ (k is Boltzmann's constant), and $\mathcal{C}$ is a constant that represents the integrated contribution of the kinetic energy and the elastic work. If one now extracts the (NEB) trajectory degree of freedom (DOF) x from the $3N$-dimensional vector $\mathbf{q}$ and separate them in Eq. (2), we have

$$G = -\frac{\mathcal{C}}{\beta}\int dx\left[\log\int d\mathbf{q}'\exp\{-\beta U(\mathbf{q}', x)\}\right]$$
$$= \int dx\,\mathcal{G}(x), \qquad (3)$$

where $U' = U(\mathbf{q}', x)$ and $\mathcal{G}(x)$ are the internal and free energies for the $(3N - 1)$ DOF system defined by generalized coordinates $\mathbf{q}'$. The force along the trajectory can be evaluated as

$$-\frac{d\mathcal{G}}{dx} = \frac{\mathcal{C}}{\beta}\frac{d}{dx}\left[\log\int d\mathbf{q}'\exp\{-\beta U(\mathbf{q}', x)\}\right]. \qquad (4)$$

The quantity $\mathcal{S}(x) = \mathcal{C}\int d\mathbf{q}'\exp\{-\beta U(\mathbf{q}', x)\}$ can be regarded as the configurational partition function of the $(3N - 1)$ DOF system, and, therefore, Eq. (4) can be written as

$$-\frac{d\mathcal{G}}{dx} = \frac{1}{\beta}\frac{d\log\mathcal{S}(x)}{dx} = \frac{1}{\beta\mathcal{S}(x)}\frac{d\mathcal{S}(x)}{dx}. \qquad (5)$$

Furthermore,

$$\frac{d\mathcal{S}(x)}{dx} = -\beta\mathcal{C}\int d\boldsymbol{q}' \exp\{-\beta U(\boldsymbol{q}', x)\}\frac{dU(\boldsymbol{q}', x)}{dx},$$

which, when inserted into Eq. (5), results in

$$\frac{d\mathcal{G}}{dx} = \frac{\int d\boldsymbol{q}' \exp\{-\beta U'\}\frac{dU'}{dx}}{\int d\boldsymbol{q}' \exp\{-\beta U'\}} = \left\langle\frac{dU'}{dx}\right\rangle, \quad (6)$$

which is a configurational average over all $(3N-1)$ DOF. In other words, the free energy of the constrained system is obtained by integrating the time-averaged total force along the minimum free energy path (see the Supplemental Material [7]).

Using Eq. (6), we now calculate free energies for the different trajectory points of the NEB calculations in our atomistic systems. Configurational averages are numerically intensive and require long simulation times to converge (on the order of several nanoseconds in our case). The resulting free energies for the unstressed configurations are shown in Fig. 3 at temperatures ranging from 100 to 600 K. G_P^h at 0, 100, and 200 K are also included for comparison. Two features are noteworthy at first glance: (i) the characteristic metastability associated with the split core configuration at 0 K is lost following constrained equilibration at finite temperatures, and (ii) the free energies suffer a marked decrease from 0 to 100 K. We find that ΔG_P vanishes completely by 700 K at zero stress. Technically, the current force field for Fe is strictly valid above the Debye temperature and below the Curie transition ($470 \lesssim T \lesssim 1040$ K). However, Proville et al. have shown that quantum effects in this context are only important below 40 K [1], and so our results over the 100–700 K temperature range are within the validity margins of the potential.

As mentioned above, the double-hump shape of the Mendelev interatomic force field as given by the NEB method is a consequence of the metastability of the split core configuration at 0 K. By contrast, DFT calculations show that the energy path displays a simpler sinusoidal profile [6,9]. Gilbert et al. have performed a detailed numerical construction of the two-dimensional energy landscape for the Mendelev potential on the {111} plane [11]. Their analysis revealed anomalies in the standard NEB path at 0 K. At finite temperatures, the system escapes the NEB path and samples a broader region of phase space until falling into an alternate dynamic path. This path is the one shown in Fig. 3 at different temperatures. This behavior explains the long convergence times and the large anharmonicities captured in Fig. 2 as the system samples alternative phase space trajectories. In any case, at 100 K, both the harmonic and full free energy curves mimic one another for $0 < x < 0.15$, which indicates that within that interval, the minimum potential and free energy paths are similar. At higher temperatures, the range of agreement gradually decreases, as more and more of the barrier is subject to anharmonic effects.

Next, we study the variation of the free energy barrier ΔG_P with temperature and stress. When $U_P(\sigma)$ displays a weak or no dependence on the stress, the dependence of Peierls enthalpy on σ is via the temperature-independent plastic work $W_p = \sigma bhx$ (per unit length). This is shown to be an accurate approximation for $\sigma < 500$ MPa (cf. Fig. 1). In such a case, one need only consider the temperature dependence of the unstressed Peierls trajectory (given in Fig. 3) and subtract W_p to obtain $G_P(\sigma; T)$. From this, ΔG_P is measured at each stress and temperature and each value plotted in Fig. 4. We term this approximation $G_P(0)$ [or $\Delta G_P(0)$ if referring to free energy barriers]. The figure reveals several interesting features. First, the free energy decreases by more than 50% from 0 to 100 K. Subsequently, it decreases gradually until it vanishes. This
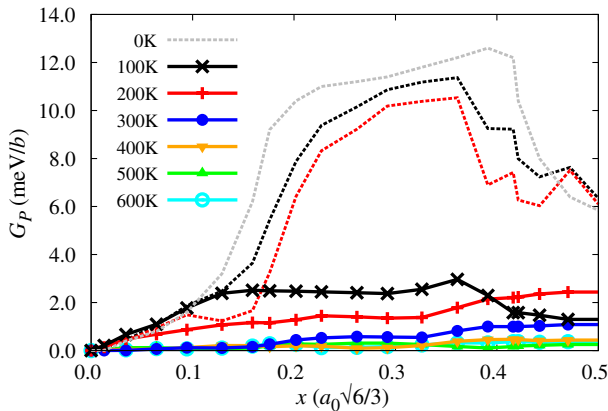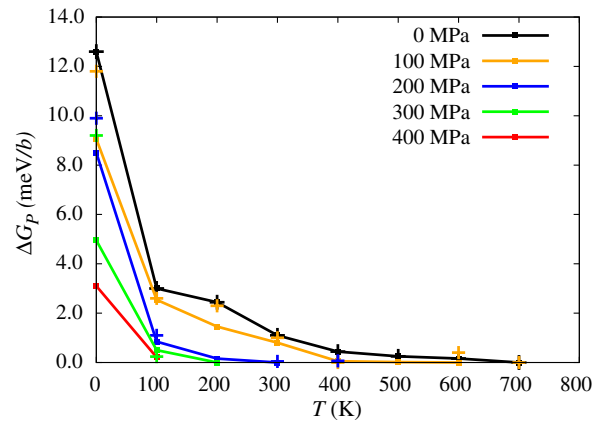

FIG. 3 (color online).   Peierls free energy path at zero stress as a function of temperature. The harmonic free energies at 100 and 200 K are also shown as dashed lines for comparison. At 700 K and above, the barrier is at or below zero.

FIG. 4 (color online).   Variation of the free energy barrier ΔG_P with temperature and stress. Solid lines correspond to $\Delta G_P(0)$, which is valid up to ≈ 400 MPa. Scatter points represent $\Delta G_P(\sigma)$, i.e., the free energies for the stress-dependent potential obtained from NEB. In the latter case, the free energy is strictly zero for $\sigma \geq 400$ MPa.
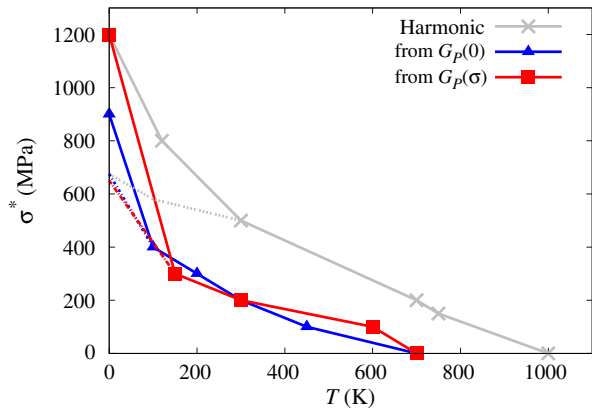
FIG. 5 (color online). Variation of the critical stress σ^* with temperature from full and harmonic free energy calculations. Solid lines represent classical calculations, whereas the dashed ones symbolize the quantum corrections at low temperature. In the classical limit, $\sigma_P \equiv \sigma^*$ at $T = 0$ K.

latter point furnishes the critical stress σ^*, i.e., that at which $\Delta G_P(\sigma^*; T) = 0$. Second, the curves at different stresses roughly mimic one another within the envelope of the zero stress results, which is an indication that the dynamic path is stable. Much in the manner of Proville *et al.* [1], adding zero-point corrections reduces the value of ΔG_P at low temperatures for all stresses. For clarity, this effect is not shown in the figure but will be taken into account when computing the critical stresses.

To verify the assumption of stress independence for the Peierls potential at 0 K below ≈ 500 MPa, we have performed free energy calculations on stressed transition paths at stresses 100 to 400 MPa. The results as a function of temperature are shown as scatter points in Fig. 4. As shown, the agreement between $\Delta G_P(0)$ and the stressed configurations $[\Delta G(\sigma)]$ is reasonable up to 300 MPa. From the data points presented in Fig. 4, we can extract the values of σ^* at each temperature. These are shown in Fig. 5, where the corresponding harmonic values are displayed for comparison. At 0 K, including zero-point motion results in $\sigma_P^q \approx 650$ MPa, which we use as a common point (joined by dashed lines) for all the curves. The critical stress vanishes at $T = 700$ K, which represents the athermal limit within our model. This is higher than experimentally observed, but our results show that the mere consideration of temperature effects leads to important changes in the dynamic picture of screw dislocations. As an example, at 100 K, $\sigma^* \approx 400$ MPa, which represents a 60% reduction with respect to the value of σ_P at 0 K.

The data provided in Fig. 5 are a central result of this Letter and reveal two main behaviors related to the Peierls potential. As referred to earlier, tensile tests in pure Fe show that the temperature dependence of the flow stress is characterized by the critical stress at (very) low temperatures (< 4 K) and the athermal limit at high temperatures. In the absence of quantum corrections, atomistic calculations,

even of the most accurate kind, fail to predict the lower temperature limit, while there is no numerical work available providing information for the higher one. The present calculations show that a formal treatment of the free energy may account for dramatic reductions in both limits using conventional interatomic force fields. Indeed, these calculations provide a closed set of data for defining a temperature-dependent substrate potential to be used in higher level models such as line tension or kinetic Monte Carlo simulations, etc. We believe the implications of this work to be of importance to all bcc metals. It is worth emphasizing that the nonsinusoidal nature of U_P from the force field employed here is not a weakening aspect of this work because finite-temperature trajectories sample paths in phase space that are not affected by the existence of the split core configuration at 0 K. This may explain why most molecular dynamics simulations of screw dislocation motion using the present interatomic potential show only correlated (in the sense of Gordon *et al.* [23]) formation of kink pairs [24,25] at finite temperatures.

To conclude, we have presented a free energy map of the $1/2\langle 111 \rangle$ screw dislocation core transition on {110} planes. The calculations have been done using constrained reaction coordinate dynamics and reveal a drastic reduction in free energy barrier and critical stress with increasing temperature. Our results can serve as yet another platform from which to interpret the discrepancies observed between atomistic simulations and macroscopic flow stress measurements.

*Corresponding author.
marian1@llnl.gov

[1] L. Proville, D. Rodney, and M.-C. Marinica, Nat. Mater. **11**, 845 (2012).
[2] D. Rodney and L. Proville, Phys. Rev. B **79**, 094108 (2009).
[3] M. Parrinello and A. Rahman, J. Appl. Phys. **52**, 7182 (1981).
[4] H. Jonsson, G. Mills, and K. Jacobsen, in *Classical and Quantum Dynamics in Condensed Phase Simulations*, edited by G.C.B.J. Berne and D.F. Coker (World Scientific, Singapore, 1998), p. 385.
[5] M.I. Mendelev, S. Han, D.J. Srolovitz, G.J. Ackland, D.Y. Sun, and M. Asta, Philos. Mag. **83**, 3977 (2003).

[6] L. Ventelon and F. Willaime, J. Comput. Aided Mater. Des. **14**, 85 (2008).

[7] See Supplemental Material http://link.aps.org/supplemental/10.1103/PhysRevLett.111.095502 for extra explanations of the methods used to calculate the core position, the harmonic free energies, and the time-averaged forces used in the free-energy integration.

[8] J. Chaussidon, M. Fivel, and D. Rodney, Acta Mater. **54**, 3407 (2006).

[9] M. Itakura, H. Kaburaki, and M. Yamaguchi, Acta Mater. **60**, 3698 (2012).

[10] L. Ventelon, F. Willaime, E. Clouet, and D. Rodney, Acta Mater. **61**, 3973 (2013).

[11] M. R. Gilbert, P. M. Derlet, and S. L. Dudarev, arXiv:1307.3848.

[12] Z. S. Basinski and J. W. Christian, Aust. J. Phys. **13**, 299 (1960).

[13] B. L. Mordike and P. Haasen, Philos. Mag. **7**, 459 (1962).

[14] H. Conrad and S. Frederick, Acta Metall. **10**, 1013 (1962).

[15] W. A. Spitzig and A. S. Keh, Acta Metall. **18**, 611 (1970).

[16] E. Kuramoto, Y. Aono, and K. Kitajima, Philos. Mag. A **39**, 717 (1979).

[17] D. Brunner and J. Diehl, Phys. Status Solidi A **124**, 155 (1991).

[18] L. Proville, L. Ventelon, and D. Rodney, Phys. Rev. B **87**, 144106 (2013).

[19] P. C. Schuck, J. Marian, J. B. Adams, and B. Sadigh, Philos. Mag. **89**, 2861 (2009).

[20] S. Rao, C. Hernandez, J. P. Simmons, T. A. Parthasarathy, and C. Woodward, Philos. Mag. A **77**, 231 (1998).

[21] E. A. Carter, G. Ciccotti, J. T. Hynes, and R. Kapral, Chem. Phys. Lett. **156**, 472 (1989).

[22] J. G. Kirkwood, J. Chem. Phys. **3**, 300 (1935).

[23] A. Gordon, T. Neeraj, Y. Li, and J. Li, Model. Simul. Mater. Sci. Eng. **18**, 085008 (2010).

[24] C. Domain and G. Monnet, Phys. Rev. Lett. **95**, 215506 (2005).

[25] M. R. Gilbert, S. Queyreau, and J. Marian, Phys. Rev. B **84**, 174103 (2011).